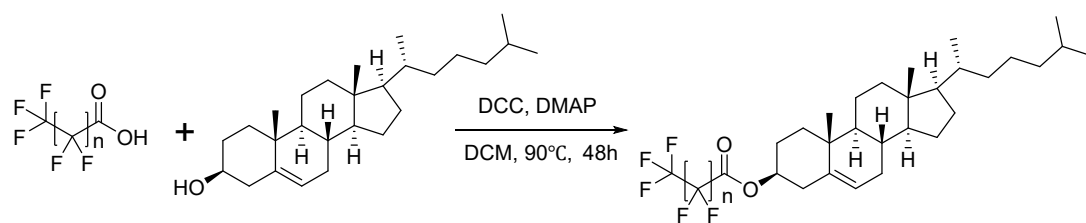


Supporting Information

**General synthesis procedure.** The synthesis process takes perfluoropropionic acid as an example, and other acids are fed with the same molar mass (Scheme S1). Cholesterol (10 mmol, 3.87g), perfluoropropionic acid (10 mmol, 1.64g), DCC (30 mmol, 6.19g) and DMAP (36 mmol, 4.4g) were dissolved in 130 mL dichloromethane in a 250 mL round-bottomed flask. Then stir the mixture at 90 °C for 48 h. Evaporate the solvent under reduced pressure and purify by silica gel column chromatography (petroleum ether: ethyl acetate = 200:1) to obtain a white solid. Unless otherwise stated, analytical grade solvents and commercially available reagents were used without further purification.



**Scheme S1.** General synthesis procedure for the series of perfluoroalkyl cholesteryl ester compounds.

**Crystal Growth.** Perfluoroalkyl cholesteryl ester compounds (5 mmol) were dissolved thoroughly in 20 mL of ethyl acetate, respectively. Then, stir the solution until clear and the colorless crystals could be obtained by solvent slow evaporation.

**Single-crystal X-ray crystallography (XRD) and Powder X-ray Diffraction (PXRD) Measurements.** Crystallographic data of CHYLP (3), CHYLH (4), CHYLN (5), CHYLU (6) and CHYLT (7) were collected using a Rigaku Saturn 924 diffractometer equipped with temperature control device, by using Cu  $K\alpha$  ( $\lambda =$

1.54184 Å) radiation. The structures of these compounds were determined and refined by Olex2 program. The data collection and structure refinement of these crystals are summarized in Table S1-S8 (CCDC number: 2322850-2322855). Powder X-ray diffraction (PXRD) data of these compounds were measured using a Rigaku D/MAX 2000 PC X-ray diffraction system with Cu K radiation in the  $2\theta$  range of  $3^\circ$ - $30^\circ$  and  $5^\circ$ - $50^\circ$  with a step size of  $0.02^\circ$  and a scan rate of  $10^\circ/\text{min}$ .

**Differential Scanning Calorimetry (DSC), Dielectric Measurements, Second Harmonic Generation (SHG) measurements and Thermogravimetric Analyses (TGA) Measurements.** DSC measurements were performed on a PerkinElmer Diamond DSC under nitrogen atmosphere in aluminum crucibles with a heating or cooling rate of  $10\text{ K/min}$ . The complex permittivity of the compounds was measured on Tonghui TH2828A during different temperature ranges. For SHG experiments, the Ins 1210058, INSTEC Instruments was used, while the laser is Vibrant 355 II, OPOTEK. By comparison with a KDP reference, the numerical values of the nonlinear optical coefficients for SHG have been determined. TGA data of these compounds were performed on PerkinElmer TGA 8000.

**UV-vis diffuse-reflectance, CD spectra measurements, IR absorbance spectra and VCD spectra.** UV-vis diffuse-reflectance spectra measurements were performed at room temperature using a Shimadzu UV-3600Plus spectrophotometer mounted with ISR-603 integrating sphere operating from 200 to 800 nm.  $\text{BaSO}_4$  was used as a 100% reflectance reference. CD spectra measurements were performed at room

temperature by JASCO J-1700 spectrometer. KBr pellet method is used for transmission mode test. The KBr tablets method was used for IR and VCD measurements. IR spectra were measured with Bruker INVENIO spectrometer equipped with PMA-50 module. The VCD spectra are recorded with Bruker INVENIO.

**Polarizing optical microscopy characterization.** The POM measurements are based on BX53-P and the temperature control device is Linkam LTS420. During the experiment, we use a magnification of  $\times 10$ .

**PFM characterization.** The PFM measurements were carried out on a commercial piezoresponse force microscope (Oxford instrument, Cypher ES) with high-voltage package at room temperature. PFM is based on the atomic force microscopy (AFM), with an AC drive voltage applied to the conductive tip. Conductive Pt/Ir-coated silicon probes (EFM, Nanoworld) were used for domain imaging and polarization switching studies, with a nominal spring constant of  $\sim 2.8$  nN/nm and a freeair resonance frequency of  $\sim 75$  kHz. The thickness of the thin film of CHYLN (5) is about  $1.5 \mu\text{m}$ .

### **Calculation condition**

The geometry optimization, vibration analysis and dipole moment were calculated at b3lyp/6-31G(d) level with Gaussian 16 software. DFT-D dispersion correction was treated with DFT-D3 method with Becke-Jonson damping<sup>1</sup>. We constructed molecular conformation based on the experimentally measured single crystal X-ray

diffraction structure. We carried out density functional calculations based on the Berry phase method developed by Kingsmith and Vanderbilt<sup>2, 3</sup>. The first-principles calculations were performed within the framework of density functional theory implemented in the Vienna ab initio Simulation Package (VASP; 5.4.4)<sup>4</sup>. The energy cut-off for the expansion of the wave functions was fixed to 550 eV and the exchange–correlation interactions were treated within the generalized gradient approximation of the Perdew–Burke–Ernzerhof type<sup>5</sup>. Van der Waals corrections are calculated based on DFT-D3 method with Becke-Jonson damping. Firstly, the geometrical optimization was performed by fixing the lattice constant based on the experimentally Xray crystal structure until the change of the total energy is smaller than 0.001. Then, the Berry phase calculation was employed based on the optimized geometry.

### **Supplementary Discussion:**

As an extension of CD into the infrared region of the spectrum, the measured vibrational circular dichroism (VCD) spectrum also confirmed the chiral feature of the crystals. The measured VCD spectrum exhibited several strong VCD signals ( $\Delta\epsilon$ ) at 1784, 1223, 1156, 1033  $\text{cm}^{-1}$  for CHYLP (3), 1779, 1233, 1224, 1218, 1209  $\text{cm}^{-1}$  for CHYLH (4), 1241, 1234, 1221 and 1020  $\text{cm}^{-1}$  for CHYLN (5), 1771, 1320, 1237, 1205, 1173  $\text{cm}^{-1}$  for CHYLU (6) and 1776, 1240, 1231, 1213  $\text{cm}^{-1}$  for CHYLT (7), respectively. These results were consistent with their absorption peaks observed in the IR spectra (Fig. S5). The calculated results showed that these VCD signals from 1223 to 1033  $\text{cm}^{-1}$  for CHYLP (3), from 1233 to 1209  $\text{cm}^{-1}$  for CHYLH (4), 1241 to 1020

$\text{cm}^{-1}$  for CHYLN (5), from 1320 to 1173  $\text{cm}^{-1}$  for CHYLU (6) and from 1240 to 1213  $\text{cm}^{-1}$  for CHYLT (7) could be mainly attributed to the C\*-C stretching vibration and C\*-H torsional vibration of the steroidal skeleton, respectively. Additionally, the VCD signals at 1784  $\text{cm}^{-1}$  for CHYLP (3), 1779  $\text{cm}^{-1}$  for CHYLH (4), 1756  $\text{cm}^{-1}$  for CHYLN (5), 1771  $\text{cm}^{-1}$  for CHYLU (6) and 1776  $\text{cm}^{-1}$  for CHYLT (7) are attributed to C=O stretching vibrations. The calculated IR and VCD spectra showed a slight peak shift compared with the measured results due to the different molecular configurations of the experiment and DFT calculation (Fig. S6).

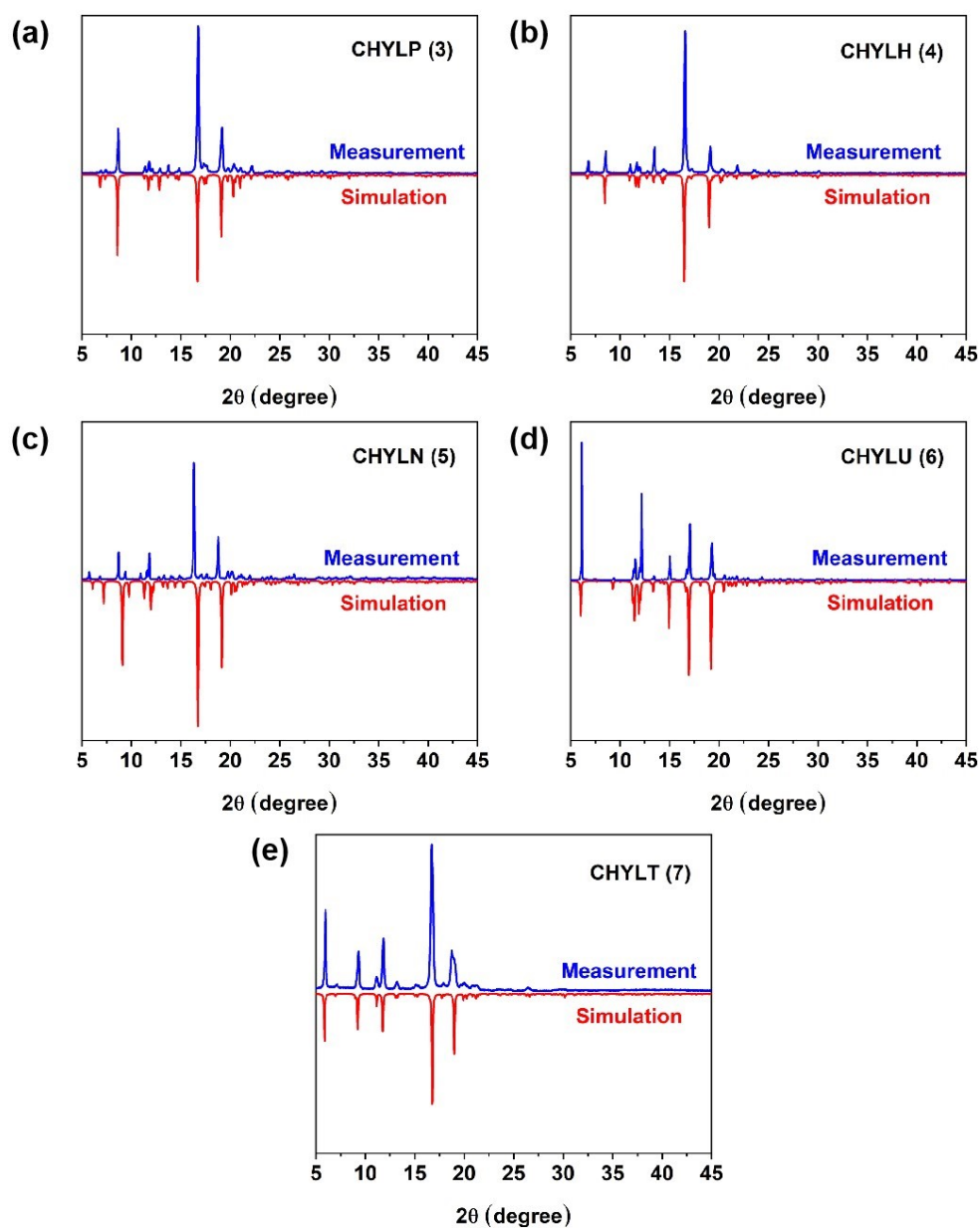


**Fig. S1** The measured powder X-ray diffraction pattern of (a) CHYLP (3), (b) CHYLH (4), (c) CHYLN (5), (d) CHYLU (6) and (e) CHYLT (7) at 298 K match well with the ones simulated by their crystal data respectively, which indicates the high phase purity.

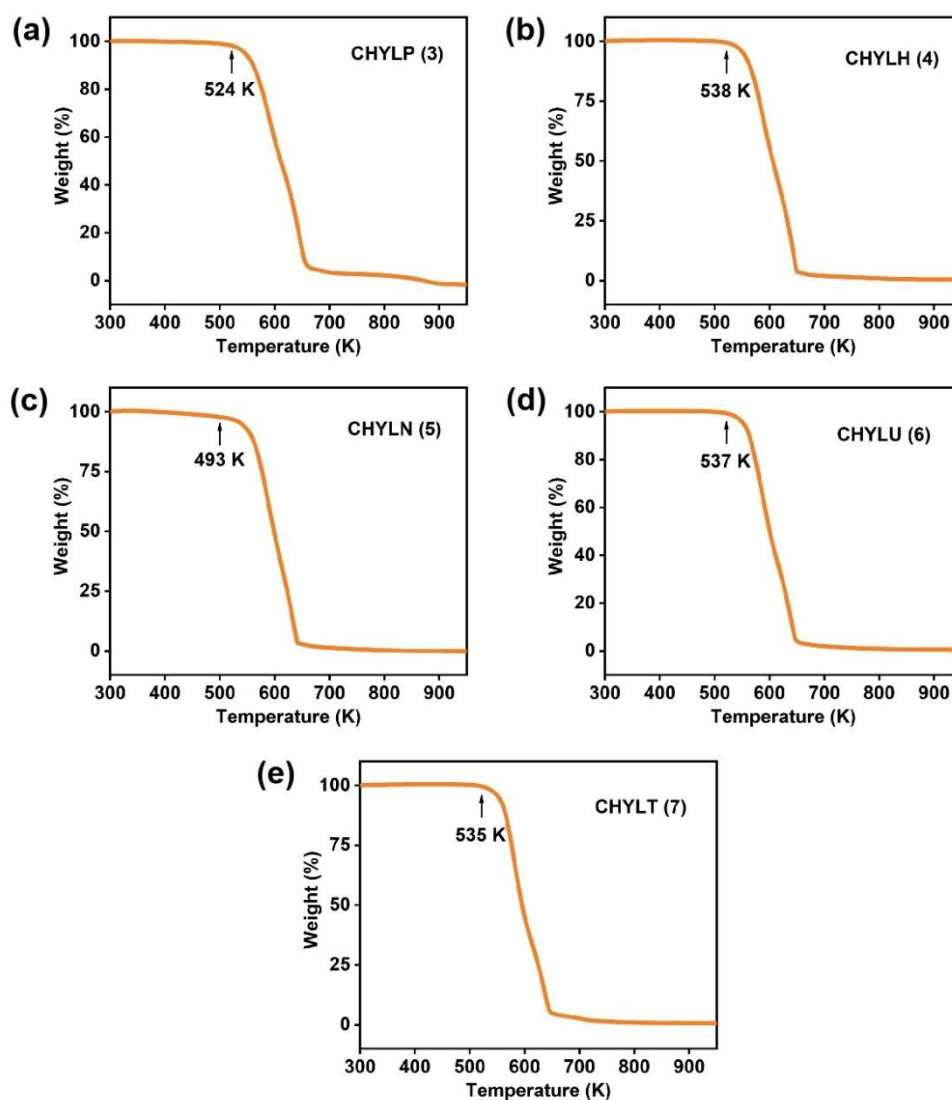


**Fig. S2** TGA curves of (a) CHYLP (3), (b) CHYLH (4), (c) CHYLN (5), (d) CHYLU (6) and (e) CHYLT (7).

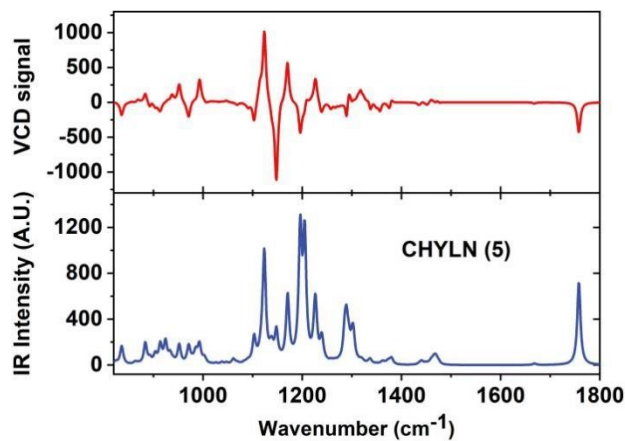


**Fig. S3** Calculated VCD and IR spectra of CHYLN (5) at b3lyp/6-31G(d) level.

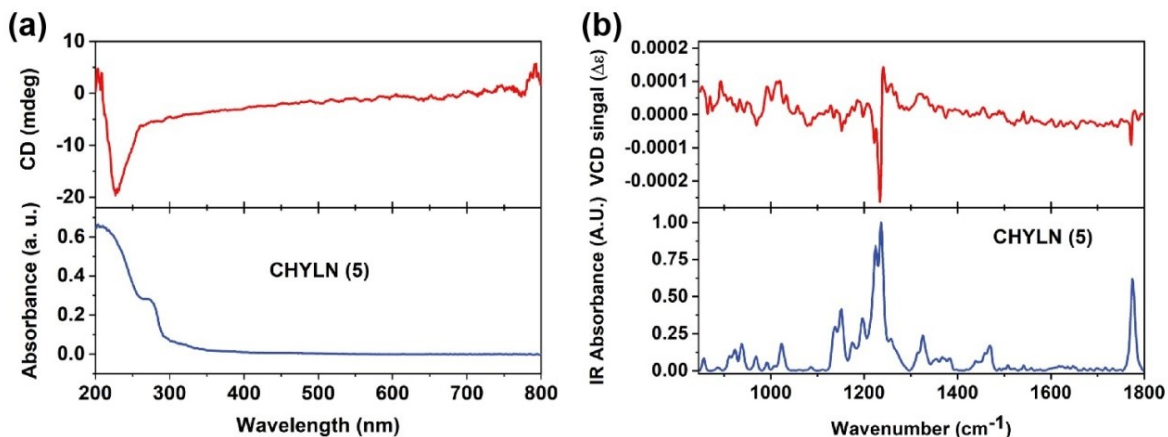


**Fig. S4** (a) Experimental measured CD and UV/Vis spectra of CHYLN (5). (b) Experimental measured VCD and IR spectra of CHYLN (5). Their chirality was demonstrated by VCD spectra, and their structure was confirmed by IR spectra at room temperature.

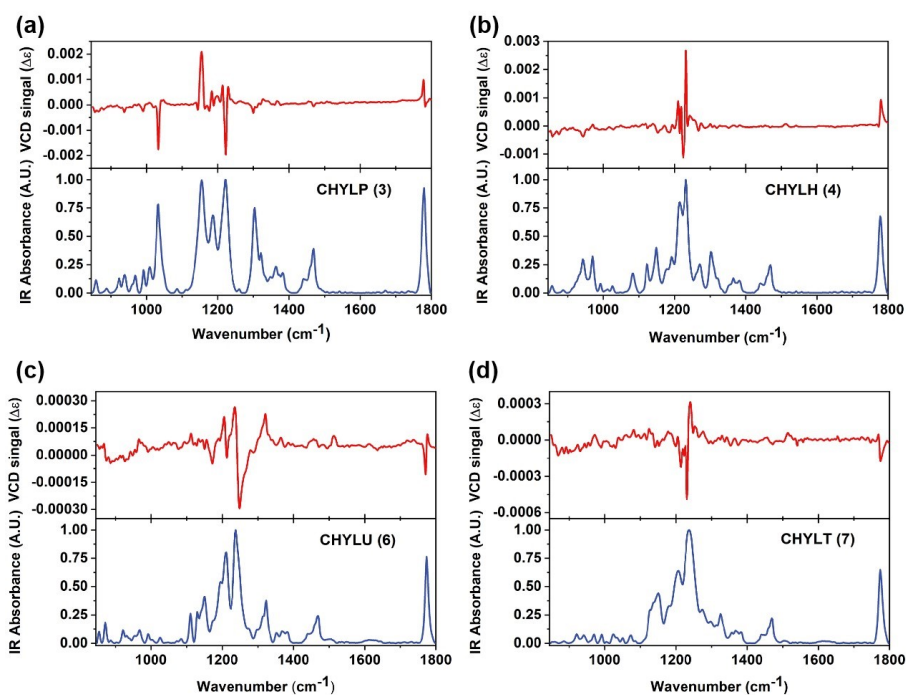


**Fig. S5** Experimental measured VCD and IR spectra of (a) CHYLP(3), (b) CHYLH(4), (c) CHYLU (6) and (d) CHYLT (7).

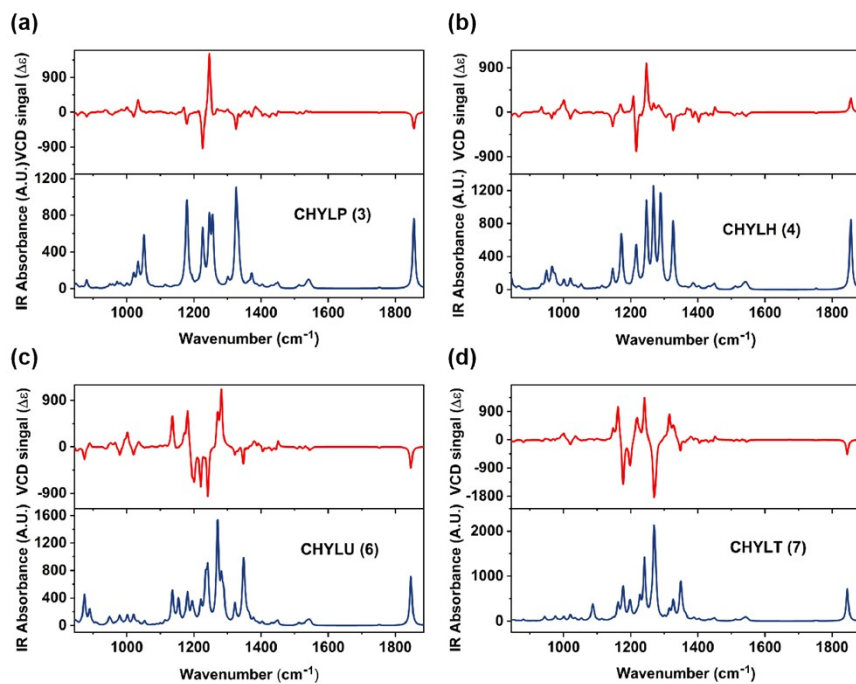


**Fig. S6** Calculated VCD and IR spectra of (a) CHYLP(3), (b) CHYLH(4), (c) CHYLU (6) and (d) CHYLT (7) at b3lyp/6-31G(d) level.

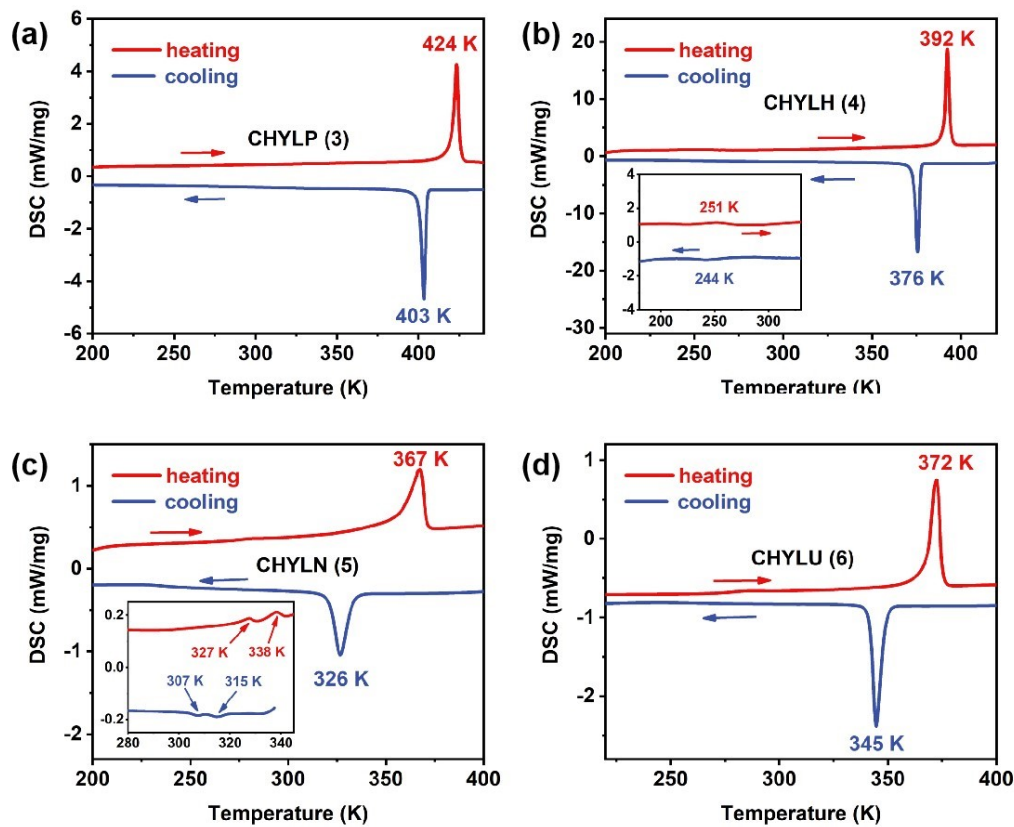


**Fig. S7** DSC curves of (a) CHYLP (3), (b) CHYLH (4) with a phase transition at 251

K, (c) CHYLN (5) with phase transitions at 327, 338 K and (d) CHYLU (6), and their melting points were determined at 424, 392, 368 and 374 K, respectively.

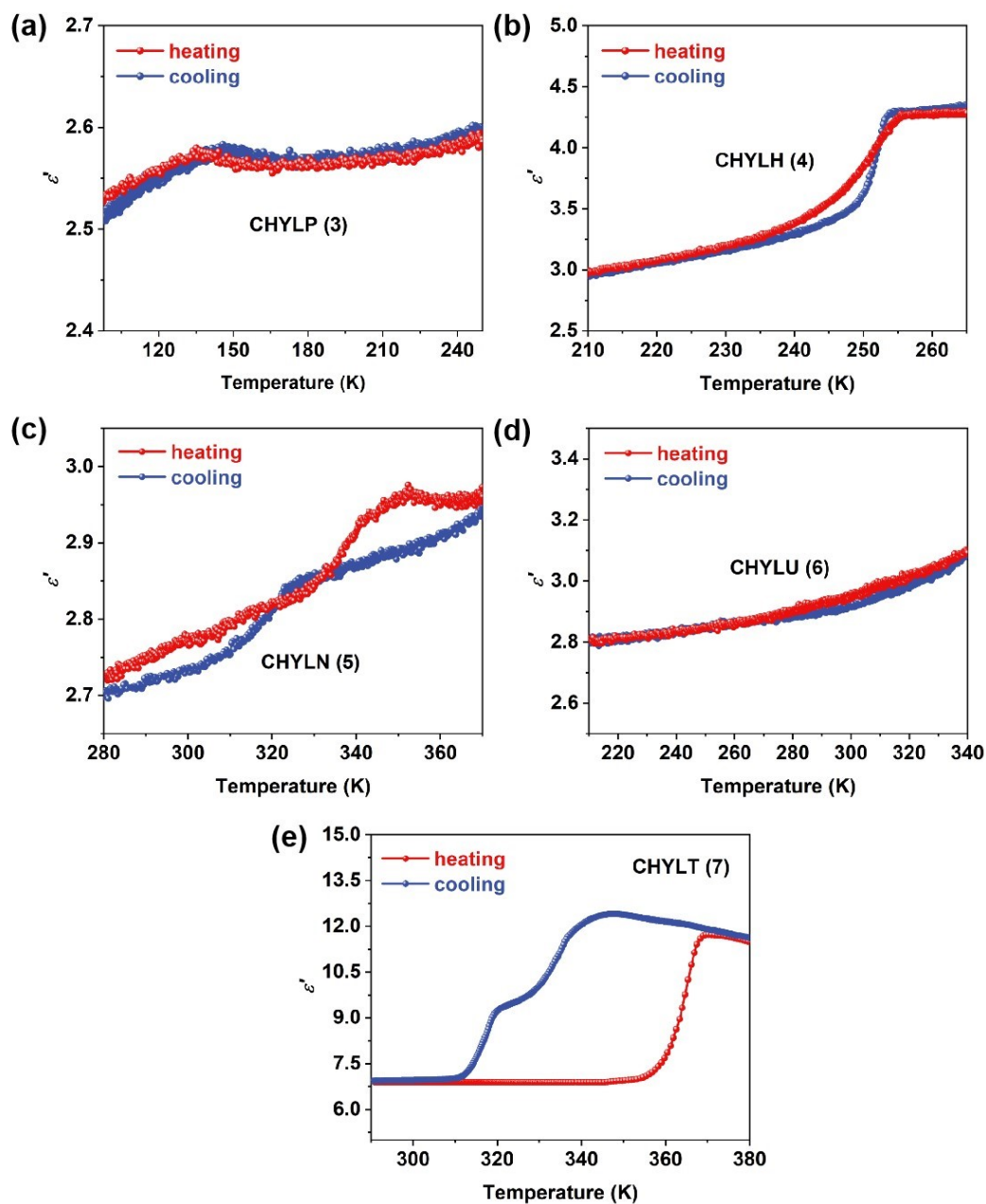


**Fig. S8** Temperature dependence of the real part of complex dielectric permittivity for compounds (a) CHYLP (3), (b) CHYLH (4), (c) CHYLN (5), (d) CHYLU (6) and (e) CHYLT (7).

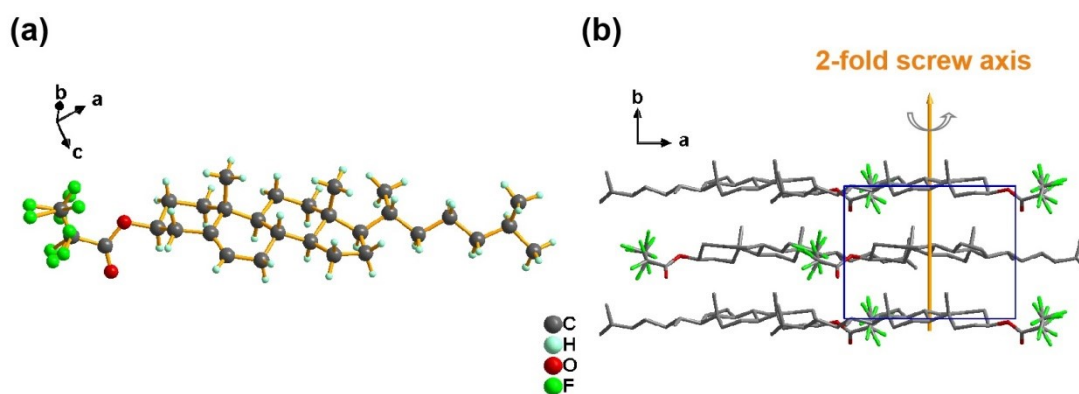


**Fig. S9** Structures of (a) CHYLP (3) in 300 K and the packing view of (b) CHYLP (3) in 300 K along the [0 0 1] direction, orange arrow symbols represent the symmetry operation of two-fold screw axes.

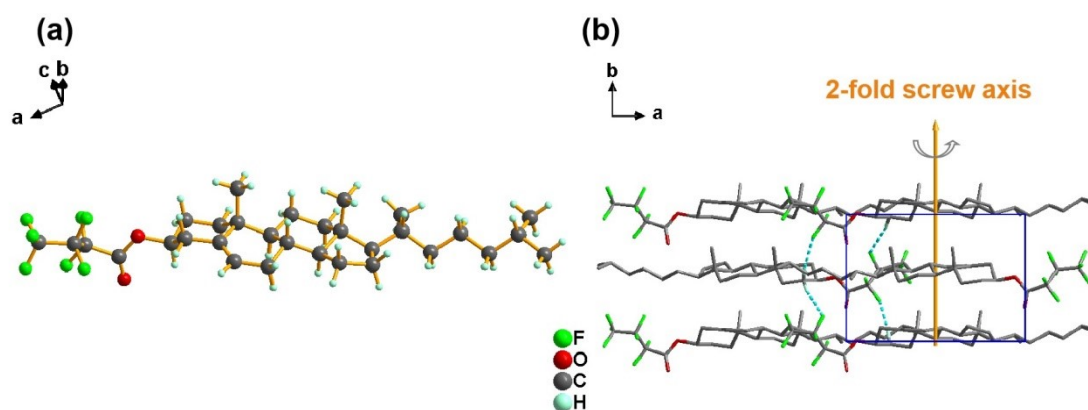


**Fig. S10** Structures of (a) CHYLH (4) in 100 K and the packing view of (b) CHYLH (4) in 100 K along the [0 0 1] direction, orange arrow symbols represent the symmetry operation of two-fold screw axis.

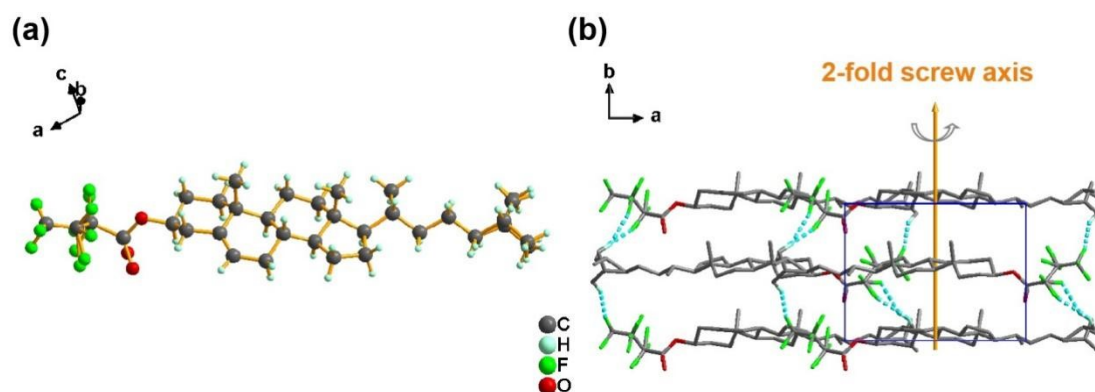


**Fig. S11** Structures of (a) CHYLH (4) in 300 K and the packing view of (b) CHYLH (4) in 300 K along the [0 0 1] direction, orange arrow symbols represent the symmetry operation of two-fold screw axis.

(4) in 300 K along the  $[0\ 0\ 1]$  direction, orange arrow symbols represent the symmetry operation of two-fold screw axis.

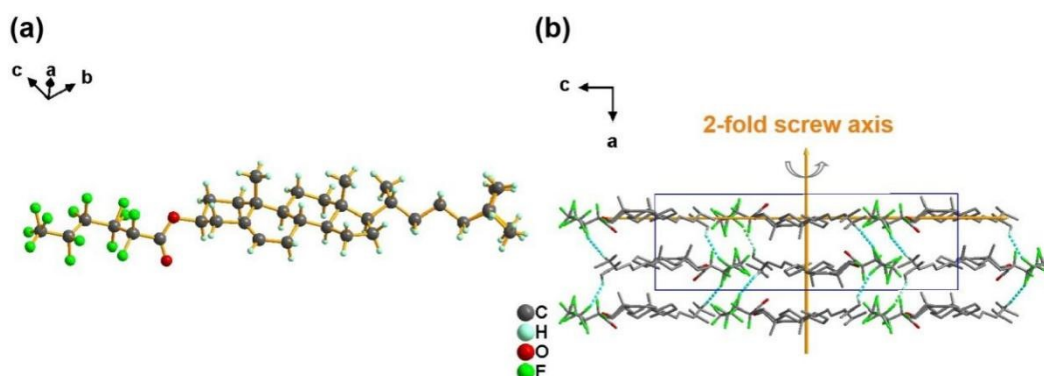


**Fig. S12** Structures of (a) CHYLU (6) in 295 K and the packing view of (b) CHYLU (6) in 295 K along the  $[0\ 1\ 0]$  direction, orange arrow symbols represent the symmetry operation of two-fold screw axis.

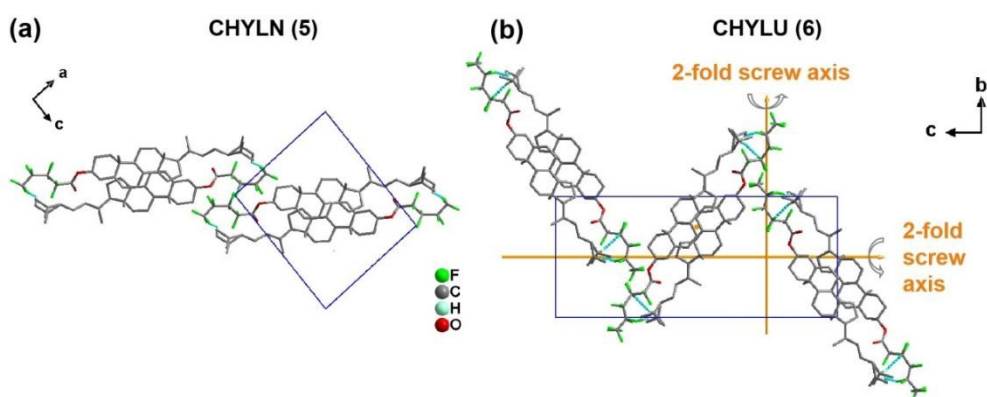


**Fig. S13** The packing view of (a) CHYLN (5) in 299 K along the  $[0\ 1\ 0]$  direction, and the packing view of (b) CHYLU (6) in 295 K along the  $[1\ 0\ 0]$  direction, orange arrow symbols represent the symmetry operation of two-fold screw axis.

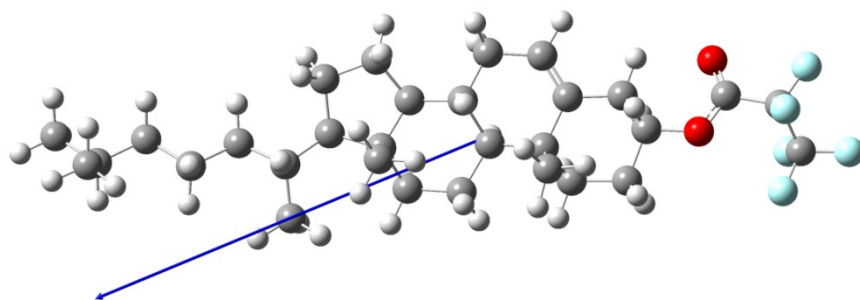


**Fig. S14** Molecular dipole of CHYLP (3) Calculated molecular configuration of CHYLP (3) with 4.02 Debye. The blue arrow indicates the dipole direction.

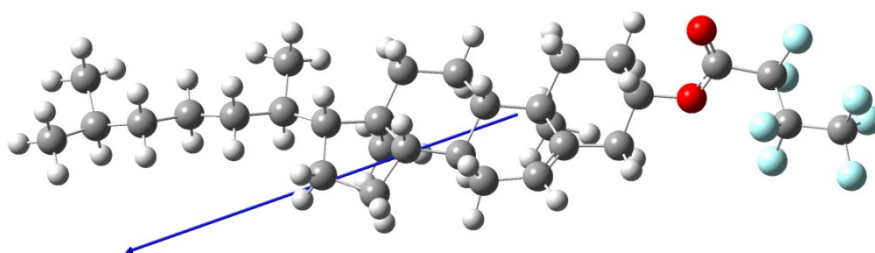


**Fig S15** Molecular dipole of CHYLH (4) Calculated molecular configuration of CHYLH (4) with 4.06 Debye. The blue arrow indicates the dipole direction.

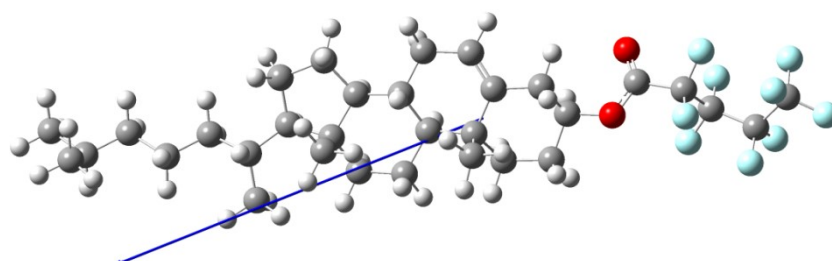


**Fig. S16** Molecular dipole of CHYLN (5) Calculated molecular configuration of CHYLN (5) with 4.13 Debye. The blue arrow indicates the dipole direction.

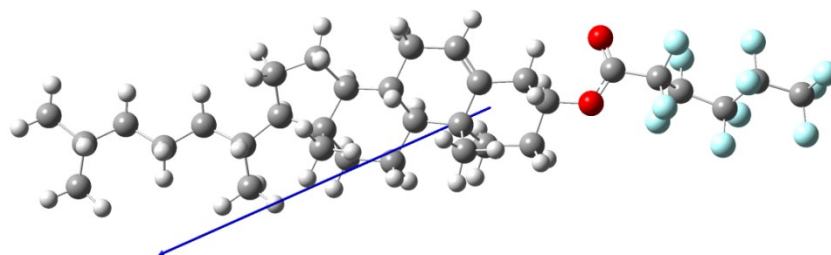


**Fig. S17** Molecular dipole of CHYLU (6) Calculated molecular configuration of CHYLU (6) with 4.13 Debye. The blue arrow indicates the dipole direction.

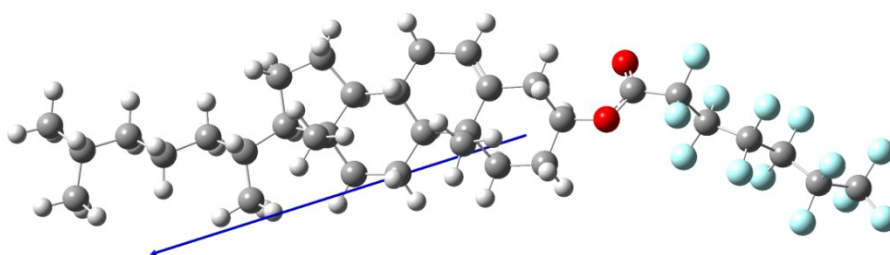


**Fig. S18** Molecular dipole of CHYLT (7) Calculated molecular configuration of CHYLT (7) with 4.13 Debye. The blue arrow indicates the dipole direction.

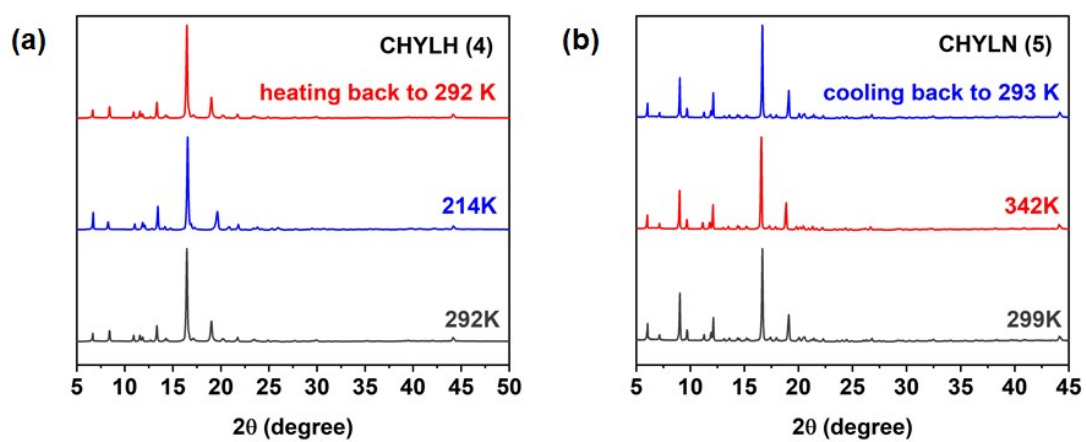


**Fig. S19** Variable-temperature PXRD patterns of (a) CHYLH (4) and (b) CHYLN (5).

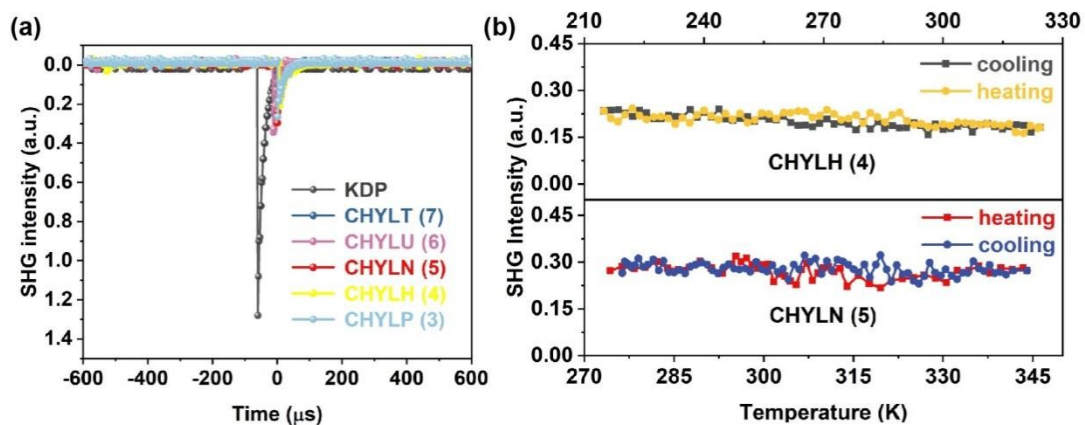


**Fig. S20** (a) The comparison of SHG signals for CHYLP (3), CHYLH (4), CHYLN (5), CHYLU (6) and CHYLT (7) crystals. (b) Temperature dependent SHG response of CHYLH (4) and CHYLN (5).

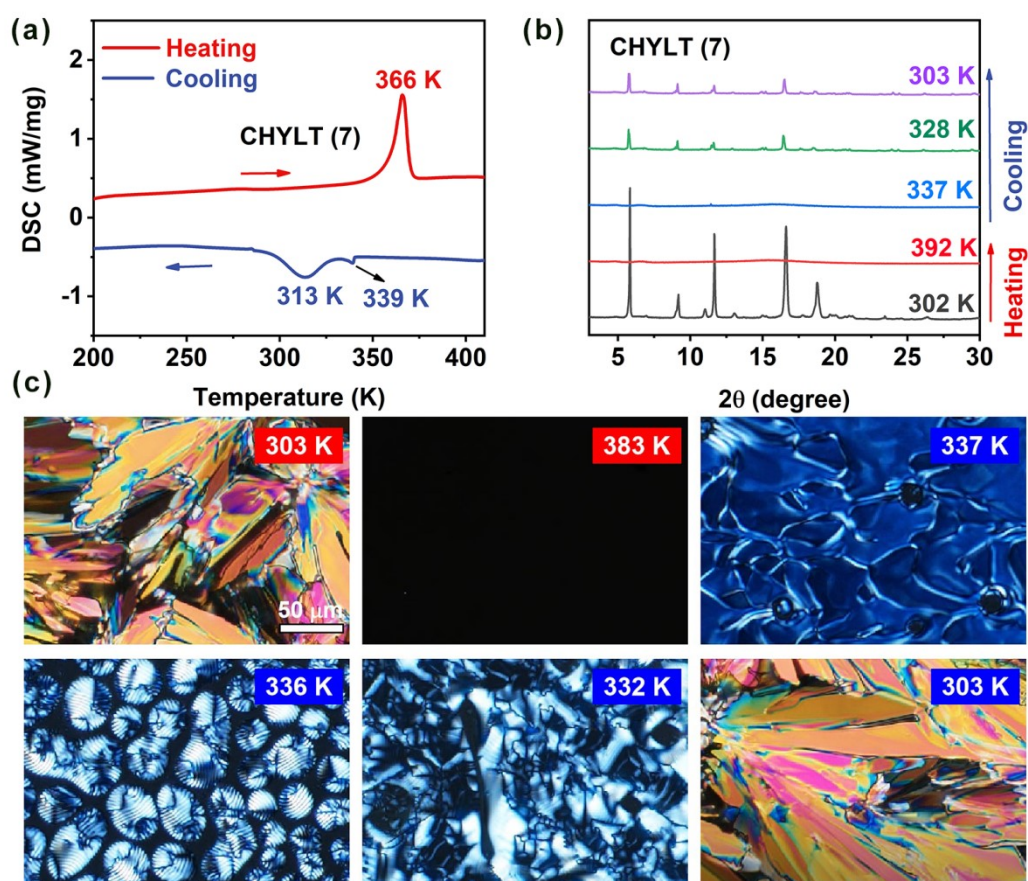


**Fig. S21** Phase transitions of CHYLT (7). (a) DSC curves of CHYLT (7). In the heating process, the phase below 366 K is SC phase, the phase above 366 K is LP

phase. In the cooling process, the phase between 313 and 399 K is the Ch phase, and the phase below 313 K is liquid LP. (b) Temperature-dependent PXRD patterns of CHYLT (7). (c) Polarized photomicrographs of CHYLT (7) in SC (303 K), LP (383 K), Ch (337, 336 and 332K).

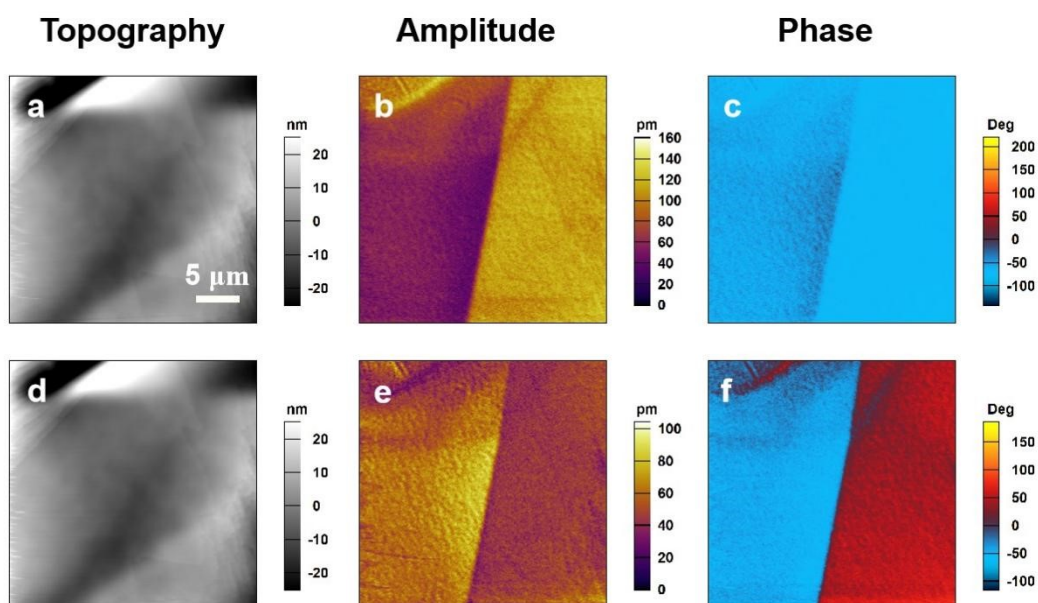


**Fig. S22** Domains observed in the CHYLT (7) thin film. (a, d) Topography, (b, e) amplitude and (c, f) phase images in lateral and vertical PFM modes. Phase signals with red and blue colors correspond to different domains, respectively.

**Table S1.** Crystal data and structure refinement for CHYLH (4) at 100K and 300 K, CHYLN (5) at 299 K, respectively.

name	CHYLH (4)		CHYLN (5)
Formula	C <sub>31</sub> H <sub>45</sub> F <sub>7</sub> O <sub>2</sub>		C <sub>32</sub> H <sub>45</sub> F <sub>9</sub> O <sub>2</sub>
Temperature	100 K	300 K	299 K
Weight	582.67	582.67	
Crystal system	monoclinic	monoclinic	monoclinic
Space group	<i>P</i> 2 <sub>1</sub>	<i>P</i> 2 <sub>1</sub>	<i>P</i> 2 <sub>1</sub>
<i>a</i> /Å	12.9607(4)	12.7803(5)	12.2990(6)
<i>b</i> /Å	8.8159(2)	9.3254(4)	9.2607(5)
<i>c</i> /Å	13.5926(4)	13.7005(7)	14.5611(9)
$\alpha$ /deg	90	90	90
$\beta$ /deg	106.421(3)	104.745(5)	94.027(5)
$\gamma$ /deg	90	90	90
Volume/Å <sup>3</sup>	1489.74(8)	1579.07(13)	1654.38(16)
<i>Z</i>	2	2	2
Density/g cm <sup>-3</sup>	1.299	1.225	1.27
<i>R</i> <sub>1</sub> [ <i>I</i> >2 $\sigma$ ( <i>I</i> )]	0.0527( 4320)	0.0781( 3938)	0.0811( 3692)
<i>wR</i> <sub>2</sub> [ <i>I</i> >2 $\sigma$ ( <i>I</i> )]	0.1430( 4409)	0.2740( 6104)	0.2563( 5354)
GOF	1.062	1.031	1.031

**Table S2.** Crystal data and structure refinement for CHYLP (3) at 300K, CHYLU (6) at 295 K and CHYLT (7) at 173 K, respectively.

name	CHYLP (3)	CHYLU (6)	CHYLT (7)
Formula	C <sub>30</sub> H <sub>45</sub> F <sub>5</sub> O <sub>2</sub>	C <sub>33</sub> H <sub>45</sub> F <sub>11</sub> O <sub>2</sub>	C <sub>34</sub> H <sub>45</sub> F <sub>13</sub> O <sub>2</sub>

Temperature	300 K	295 K	173 K
Weight	532.66	682.69	732.70
Crystal system	monoclinic	orthorhombic	monoclinic
Space group	$P2_1$	$P2_12_12_1$	$P2_1$
$a/\text{\AA}$	12.4586(2)	9.2360(4)	13.3455(3)
$b/\text{\AA}$	9.2797(2)	12.5420(4)	8.8735(2)
$c/\text{\AA}$	13.4386(3)	29.3792(10)	14.4040(3)
$\alpha/\text{deg}$	90	90	90
$\beta/\text{deg}$	105.661(2)	90	90.499(2)
$\gamma/\text{deg}$	90	90	90
Volume/ $\text{\AA}^3$	1495.99(5)	3403.2(2)	1705.68(6)
Z	2	4	2
Density/ $\text{g cm}^{-3}$	1.182	1.332	1.427
$R_1 [I > 2\sigma(I)]$	0.0577( 4941)	0.0817( 4820)	0.0478( 5980)
$wR_2 [I > 2\sigma(I)]$	0.1840( 5674)	0.2702( 6256)	0.1425( 6755)
GOF	1.075	1.057	1.065

**Table S3.** Hydrogen Bonds for CHYLP (3) at 300K.

D	H	A	d(D-H)/ $\text{\AA}$	d(H-A)/ $\text{\AA}$	d(D-A)/ $\text{\AA}$	D-H-A/ $^\circ$
C005	H00E	F11 <sup>1</sup>	0.97	2.74	3.442(9)	129.9
C00K	H00X	F3 <sup>2</sup>	0.97	2.82	3.514(15)	129.2
C00M	H00Z	O00I	0.98	2.38	2.710 (6)	99.1
C00T	H3	O00I	0.97	3.11	3.456(8)	102.9
C010	H01C	F7 <sup>3</sup>	0.96	2.71	3.59(2)	152.5

<sup>1</sup>1+X, +Y, 1+Z; <sup>2</sup>1-X, -1/2+Y, 1-Z; <sup>3</sup>1-X, 1/2+Y, 1-Z

**Table S4.** Hydrogen Bonds for CHYLH (4) at 100K.

D	H	A	d(D-H)/Å	d(H-A)/Å	d(D-A)/Å	D-H-A/°
C22	H22	F32 <sup>1</sup>	1.00	2.92	3.595(4)	125.9
C9	H9B	F34 <sup>2</sup>	0.99	2.95	3.486(4)	115.4
C8	H8A	F38 <sup>3</sup>	0.99	2.50	2.479 (5)	170.0
C8	H8B	F34 <sup>2</sup>	0.99	2.89	3.592(5)	129.0
C12	H12	F36 <sup>4</sup>	0.99	2.69	3.594(4)	151.8
C7	H7	O39	1.00	2.37	2.747(5)	101.3
C23	H23A	F38 <sup>1</sup>	0.98	2.69	3.516(5)	142.2
C23	H23B	F32 <sup>1</sup>	0.98	2.97	3.303(5)	100.9
C23	H23C	F32 <sup>5</sup>	0.98	3.02	3.491(4)	110.7
C23	H23C	F33 <sup>6</sup>	0.98	2.68	3.533(5)	146.0

<sup>1</sup>-3-X, 1/2+Y, 1-Z; <sup>2</sup>-2-X, -1/2+Y, 2-Z; <sup>3</sup>-2-X, 1/2+Y, 2-Z; <sup>4</sup>-1+X, +Y, +Z; <sup>5</sup>-3-X, -1/2+Y, 1-Z; <sup>6</sup>-3-X, -1/2+Y, 1-Z

**Table S5.** Hydrogen Bonds for CHYLH (4) at 300K.

D	H	A	d(D-H)/Å	d(H-A)/Å	d(D-A)/Å	D-H-A/°
C00O	HA	O16	0.97	2.93	3.34(2)	107.0
C00W	H4	O00S	0.98	2.34	2.714(18)	101.7
C00W	H4	O16	0.98	2.36	2.710 (15)	100.1
C16	H16	F3 <sup>1</sup>	0.96	2.69	3.51(4)	142.9
C5	H5A	F2 <sup>2</sup>	0.96	1.97	2.82(3)	146.8
C5	H5B	F3 <sup>3</sup>	0.96	2.73	3.25(2)	115.1

<sup>1</sup>-1-X, 1/2+Y, -1-Z; <sup>2</sup>-1-X, -1/2+Y, -1-Z; <sup>3</sup>-2+X, +Y, -1+Z

**Table S6.** Hydrogen Bonds for CHYLN (5) at 299K.

D	H	A	d(D-H)/Å	d(H-A)/Å	d(D-A)/Å	D-H-A/°
C008	H00C	F00J <sup>1</sup>	0.97	3.01	3.495(6)	112.1
C00H	H00N	O00S	0.98	2.39	2.707(8)	97.9
C00W	H3	O00S	0.97	3.00	3.385 (10)	104.9
C3	H3A	F3 <sup>2</sup>	0.96	2.62	3.21(3)	120.3

<sup>1</sup>-1+X, +Y, +Z; <sup>2</sup>-1-X, -1/2+Y, -1-Z

**Table S7.** Hydrogen Bonds for CHYLU (6) at 295K.

D	H	A	d(D-H)/Å	d(H-A)/Å	d(D-A)/Å	D-H-A/°
C30	H30A	F33 <sup>1</sup>	0.97	2.79	3.509(8)	131.7
C1	H1	F27 <sup>2</sup>	0.98	2.61	3.573(16)	167.9
C5	H5B	F31 <sup>3</sup>	0.96	2.82	3.44 (4)	122.7
C11	H11B	F5 <sup>4</sup>	0.96	2.58	3.25(3)	127.4

<sup>1</sup>+X, 1+Y, +Z; <sup>2</sup>1/2+X, 3/2-Y, 1-Z; <sup>3</sup>1/2-X, 2-Y, -1/2+Z; <sup>4</sup>-1/2+X, 3/2-Y, 1-Z

**Table S8.** Hydrogen Bonds for CHYLT (7) at 173K.

D	H	A	d(D-H)/Å	d(H-A)/Å	d(D-A)/Å	D-H-A/°
C00H	H00B	F004 <sup>1</sup>	0.99	2.68	3.417(4)	131.2
C00H	H00B	F00E <sup>1</sup>	0.99	3.09	3.582(5)	112.3
C00O	H00C	F002 <sup>2</sup>	0.99	3.14	3.521(5)	104.6
C00O	H00C	F008 <sup>2</sup>	0.99	2.97	3.533(4)	116.9
C00P	H00E	F00A <sup>3</sup>	0.99	2.65	3.489(4)	143.2
C00P	H00F	F004 <sup>3</sup>	0.99	3.20	3.583(4)	104.7
C00U	H00U	F004 <sup>1</sup>	1.00	2.89	3.398(4)	112.6

C00U	H00U	O00F	1.00	2.52	2.755(4)	92.6
C010	H01B	O00F	0.99	2.78	3.253(5)	110.0
C011	H01C	F002 <sup>2</sup>	0.99	2.73	3.500(3)	135.0
C013	H013	F007 <sup>4</sup>	1.00	2.54	3.327(4)	135.3
C016	H01E	F6 <sup>5</sup>	0.99	2.92	3.531(5)	120.8
C01C	H01R	F00D <sup>6</sup>	0.98	2.77	3.423(5)	124.3
C01D	H01T	F5 <sup>3</sup>	0.98	2.62	3.549(5)	157.7
C01D	H01U	F007 <sup>4</sup>	0.98	2.93	3.305(6)	103.7

<sup>1</sup>-X, -1/2+Y, -Z; <sup>2</sup>1+X, +Y, +Z; <sup>3</sup>1+X, +Y, 1+Z; <sup>4</sup>1-X, 1/2+Y, 1-Z; <sup>5</sup>1-X, -1/2+Y, 1-Z;

<sup>6</sup>-X, 1/2+Y, -Z

- [1] Grimme, S.; Ehrlich, S.; Goerigk, L., Effect of the damping function in dispersion corrected density functional theory. *J. Comput. Chem.* **2011**, *32* (7), 1456-1465.
- [2] King-Smith, R. D.; Vanderbilt, D., Theory of polarization of crystalline solids. *Phys. Rev. B* **1993**, *47* (3), 1651-1654.
- [3] Vanderbilt, D.; King-Smith, R. D., Electric polarization as a bulk quantity and its relation to surface charge. *Phys. Rev. B* **1993**, *48* (7), 4442-4455.
- [4] Kresse, G.; Furthmüller, J., Efficient iterative schemes for ab initio total-energy calculations using a plane-wave basis set. *Phys. Rev. B* **1996**, *54* (16), 11169-11186.
- [5] Kresse, G.; Furthmüller, J., Efficiency of ab-initio total energy calculations for metals and semiconductors using a plane-wave basis set. *Comput. Mater. Sci.* **1996**, *6* (1), 15-50.